Adsorption Properties of Templated Mesoporous Carbon (CMK-1) for Nitrogen and Supercritical Methane—Experiment and GCMC Simulation

Takahiro Ohkubo,[†] Jin Miyawaki,[†,‡] and Katsumi Kaneko*[,†,§]

Graduate School of Natural Science and Technology, and Center for Frontier Electronics and Photonics, Chiba University, 1-33 Yayoi, Inage, Chiba 263-8522, Japan

Ryong Ryoo

National Creative Research Initiative Center for Functional Nanomaterials and Department of Chemistry (School of Molecular Science-BK21), Korea Advanced Institute of Science and Technology, Taejon, 305-701, Korea

Nigel A. Seaton

School of Chemical Engineering, King's Building, University of Edinburgh, Mayfield Road, Edinburgh EH9 3JH, United Kingdom

Received: January 9, 2002

Nitrogen adsorption isotherms at 77 K and high pressure adsorption of supercritical methane at 303 K were measured on mesoporous carbon (CMK-1) prepared from the templating of MCM-48. These experimental isotherms were simulated with grand canonical Monte Carlo (GCMC) simulation using the rod-aligned slitlike pore (RSP) model. This RSP model gives good agreement with the experimental nitrogen adsorption isotherm in the low-pressure region, while it describes well the observed methane isotherm. The isothermal compressibility of the adsorbed methane at 303 K was calculated from the experimental and simulated isotherms. The isothermal compressibility of the adsorbed methane shows the intermediate state between the supercritical and liquid phase. This indicates that the adsorbed layer of supercritical methane is highly compressed by the strong interaction potential from the pore walls.

Introduction

The molecular adsorption technique has been applied to gas storage, adsorptive separation, and purification.[1] Especially, the gas storage in micropores of carbon has been interesting from the industrial point of view, because these carbon materials are prospective adsorbents for storage of hydrogen and methane,[2,3] which are indispensable fuel gases in future. In addition, porous carbon has another application in supercapacitors, which can contribute to new energy systems.[4] We have already published that the molecules adsorbed in carbon micropores tend to form a highly ordered structure depending on the pore width and properties of adsorbate molecules by in situ X-ray diffraction (XRD).[5−10] Thus, elucidation of the pore structures of prospective porous carbon adsorbents and molecular states in pores is required.

Recently, a variety of solids having regular pore structure have been developed. As it is difficult to control the pore size of porous carbons with traditional activation procedures, a new preparation method of porous carbons must be developed. Templating synthesis is a quite hopeful method. Kyotani et al. produced carbon tubes whose pores belong to large mesopores with the aid of the aluminum oxide template.[11] Ryoo et al. succeeded in the preparation of mesoporous carbons, which are named CMK-n ($n = 1-5$),[12−17] using the mesoporous silica as the template. One of the CMK-type carbons (CMK-1)[12] templated by MCM-48[18] has three-dimensional periodic regular pore structures revealed by high-resolution transmission electron microscope (HRTEM) and XRD measurements. However, the pore structure of CMK-1 is nevertheless complex compared with ordinary zeolites and carbon nanotubes. As the high potential of CMK-1 as a new adsorbent has been expected, a more exact understanding of the relationship between the pore structure and adsorption mechanism in the pores is necessary. The grand canonical Monte Carlo (GCMC) simulation technique[19] has been devoted to unveil the molecular adsorption mechanism in pores and to characterize the pore structures. Hence a GCMC simulation study with appropriate experiments should elucidate the pore structures of CMK-1 and the adsorbed states of molecules in the pores.

In this paper, we determine the adsorption isotherms of nitrogen and methane on CMK-1 and simulated these adsorption isotherms using a rod-aligned slitlike pore (RSP) model by use of GCMC technique.

RSP Model and GCMC Simulation. Although the HRTEM study showed a high alignment of rodlike structures, the true channel structure is not simple and the channels have a kind of textural structure.[12] As molecular adsorption depends sensitively on the interaction potential between a molecule and the solid pore wall, an optimum model must contain a geometrical feature having a strong interaction potential, if we cannot use the real atomic structure for the GCMC simulation. Figure 1 shows the carbon RSP model that is close to the HRTEM image structure and some definitions of parameters used in the simulation. Here the carbon rod consists of five coaxial cylinders of the graphene sheet and the inter-sheet distance was taken from the value of graphite (0.3354 nm). Therefore, the largest diameter of a carbon

* Corresponding author.
[†] Graduate School of Natural Science and Technology, Chiba University.
[‡] Present address: The Energy Institute, The Pennsylvania State University, 401 Academic Activities Building, University Park, Pennsylvania 16802-2308.
[§] Center for Frontier Electronics and Photonics, Chiba University.

10.1021/jp0200369 CCC: $22.00
Published on Web 06/01/2002

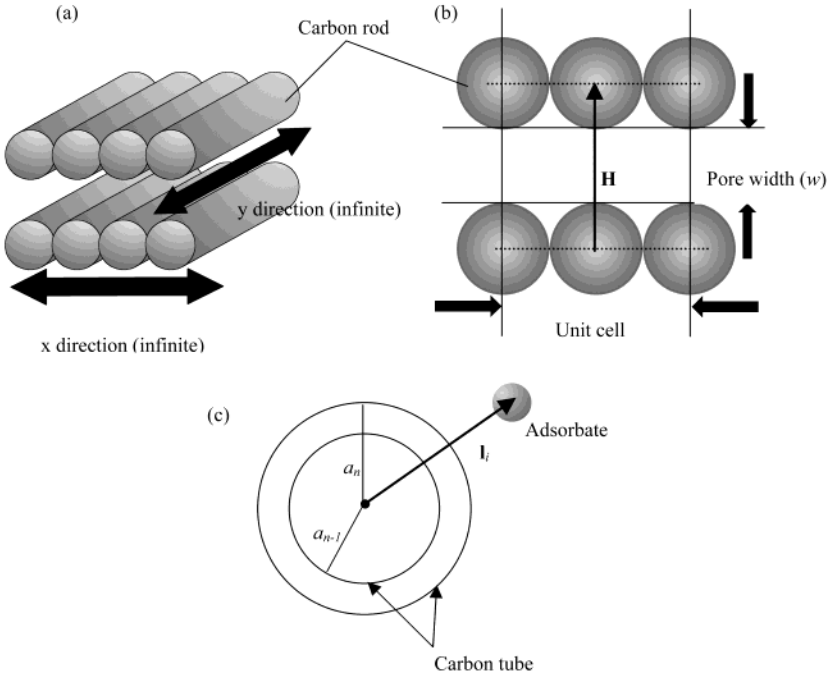

Figure 1. Schematic illustrations of the RSP model used in this work and some definitions of parameters in GCMC simulation.

rod was 3.164 nm, i.e., a size similar to the pore width of MCM-48.[20] This RSP model expresses the characteristic grooved structure of CMK-1, which should affect sensitively the gas adsorption property. Hence, we simulated the nitrogen and methane adsorption isotherms using GCMC technique for RSP model.

The intermolecular interaction between the adsorbed molecules ($\phi_{ff}(r_{ij})$) is modeled using Lennard-Jones (LJ) potential:

$$\phi_{ff}(r_{ij}) = 4\epsilon_{ff}\left[\left(\frac{\sigma_{ff}}{r_{ij}}\right)^{12} - \left(\frac{\sigma_{ff}}{r_{ij}}\right)^{6}\right] \tag{1}$$

Here, r_{ij} is the intermolecular separation and ϵ_{ff} and σ_{ff} are LJ parameters of fluids. Table 1 shows LJ parameters of nitrogen and methane used in this work. The interaction potential of an adsorbed fluid with the surfaces of RSP model is described by a summation of the interaction potential of an adsorbed fluid with a carbon cylinder ($\upsilon_{sf}(l_i)$).[21]

$$\upsilon_{sf}(l_i)) = 4\rho_{2-C}\epsilon_{sf}\sum_{n=1}^{5}({\sigma_{sf}}^{12}I_{12} - {\sigma_{sf}}^{6}I_6)$$

$$I_{12} = \frac{63\pi^2(a_n/l_i)^{11}}{128{a_n}^{10}\{1-(a_n/l_i)^2\}^{10}}F\left(-\frac{9}{2}, -\frac{9}{2};1;(a_n/l_i)^2\right)$$

$$I_6 = \frac{3\pi^2(a_n/l_i)^5}{4{a_n}^4\{1-(a_n/l_i)^2\}^4}F\left(-\frac{3}{2}, -\frac{3}{2};1;(a_n/l_i)^2\right) \tag{2}$$

Here ρ_{2-C} is a two-dimensional density of a carbon cylinder, a_n is the radius of the carbon cylinder consisting of the nth layer, l_i is the distance from the center line of a carbon rod to an adsorbed molecule, and F is a hypergeometric function, and σ_{sf} and ϵ_{sf} are the size and energy parameters in the LJ potential between an adsorbed molecule and a carbon atom which were calculated by the Lorentz−Berthelot rules using the parameter values shown in Table 1. The total adsorbate−adsorbent interaction potential for the RSP model (ϕ_{sf}) is obtained by summing the interactions between the fluid molecule and the carbon rod.

TABLE 1: Values of Lennard-Jones and Adsorbent Parameters Used in the Simulations

parameter[a]	value
nitrogen	
σ_{ff}	0.3549 nm
ϵ_{ff}/k_B	94.95 K
methane	
σ_{ff}	0.3810 nm
ϵ_{ff}/k_B	148.2 K
carbon (adsorbent)	
σ_{ss}	0.340 nm
ϵ_{ss}/k_B	28.0 K
ρ_{2-C}	38.2 nm^{-2}
ρ_{3-C}	114.0 nm^{-3}
Δ	0.3354 nm

[a] k_B is the Boltzmann constant.

$$\phi_{sf} = \sum_{i=1}^{3}[\upsilon_{sf}(|\mathbf{l}_i|) + \upsilon_{sf}(|\mathbf{l}_i - \mathbf{H}|)] \tag{3}$$

Here $\mathbf{l}_i$ is a normal vector from a center line of one carbon cylinder to an adsorbed molecule (i.e., $l_i = |\mathbf{l}_i|$) and $\mathbf{H}$ is also a normal vector between the plates which are constructed by the center lines of carbon cylinders of one side, as shown in Figure 1b. The space between the three parallel rods was used as the unit cell for simulation.

The types of Monte Carlo steps involved in a GCMC simulation are moves, creations, and destructions. In each step either a move, creation, or destruction was attempted with equal probability. For each isotherm point the system was allowed to equilibrate over 100 000 steps. After equilibration the simulation continued for over 2 000 000 steps for each isotherm point. The absolute adsorption isotherms were obtained and, in the case of nitrogen adsorption isotherms, these were converted into excess adsorption isotherms by using the pore volume in a RSP

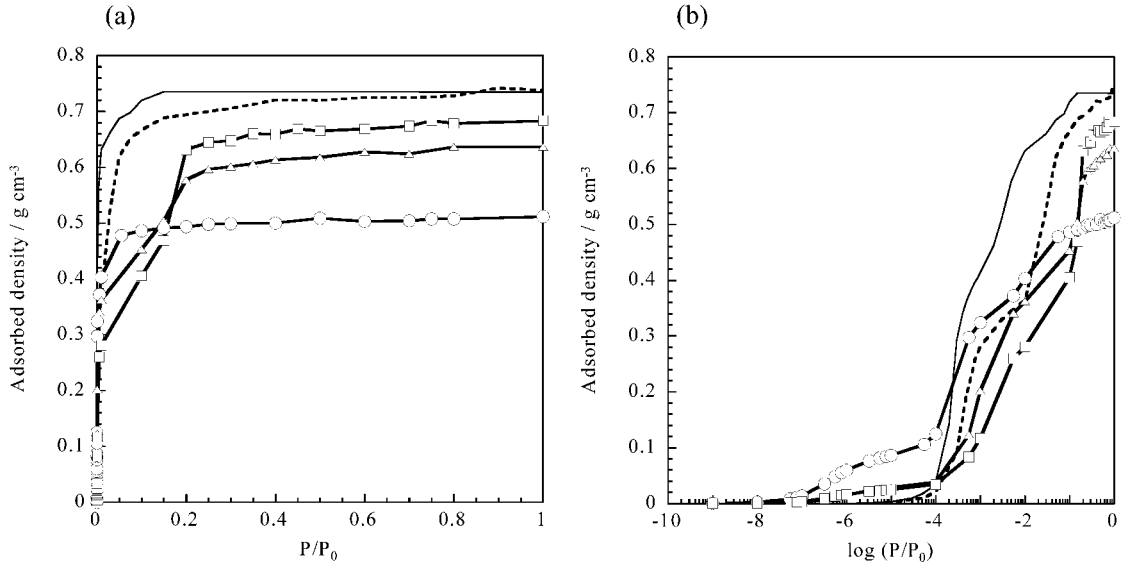

Figure 2. Calculated adsorption isotherms of nitrogen on the RSP model at 77 K: (○) $w = 0.264$ nm; (△) $w = 0.764$ nm; (□) $w = 1.264$ nm. Here the abscissa of Figure 2b is represented by the logarithm scale. The calculated isotherms on slit-shaped model pore of $w = 0.96$ nm (solid line) and 1.36 nm (dashed line) are also shown for comparison.

model and Peng-Robinson equation of state (EOS).[22] The parameters used in the EOS were those quoted by Sandler.[23]

Experimental Section

CMK-1 was synthesized by the same method as described in the literature.[12] The high-resolution nitrogen adsorption isotherm was measured at 77 K using a gravimetric method. The sample was preevacuated at 10 mPa and 383 K for 2 h. The micropore structural parameters were obtained from high-resolution α_s-plot analysis of the nitrogen adsorption isotherm in a way similar to those of preceding papers.[24,25] The adsorption isotherm of methane on CMK-1 was measured at 303 K using the method reported by Miyawaki et al.[3] The high-pressure adsorption isotherm was converted to an absolute adsorbed amount isotherm by a buoyancy mediated (BM) method[26] to compare with the simulated absolute amount.

Results and Discussion

Nitrogen Adsorption Mechanism. The calculated adsorption isotherms of nitrogen for the RSP model at 77 K for different pore widths are shown in Figure 2. In this figure, the effective pore width w is defined as a minimum effective pore width between the aligned sheets, which is obtained by using the relation, involved in a previous paper.[27] These values are determined with eq 4:

$$w = |\mathbf{H}| - 2a_5 - (2z_0 - \sigma_{ff})z_0 = 0.850\sigma_{sf} \qquad (4)$$

In Figure 2, two simulated adsorption isotherms of nitrogen on a slit-shaped carbon pore at 77 K are also shown for comparison. These two isotherms for slit pores of $w = 0.96$ and 1.36 nm show representative features of the isotherms for other w values. The simulated isotherms of $w < 0.96$ nm have an almost vertical rise below $P/P_0 = 10^{-4}$. Also the greater the w value, the clearer the two-step nature of the isotherm in the w range of 1 to 2 nm. Hence, the simulated isotherm of $w = 1.36$ nm is presented as one of the representative two-step isotherms for the slit pores. These isotherms were calculated with the Steele's 10-4-3 potential that is a function of the interaction between an adsorbed molecule and a flat graphite surface ($\phi_{sf}(z)$):[28]

$$\phi_{sf}(z) = A\left[\frac{2}{5}\left(\frac{\sigma_{sf}}{z}\right)^{10} - \left(\frac{\sigma_{sf}}{z}\right)^{4} - \frac{{\sigma_{sf}}^4}{3\Delta(z + 0.61\Delta)^3}\right] \qquad (5)$$

$$A = 2\pi{\sigma_{sf}}^2\epsilon_{sf}\rho_{3-C}\Delta$$

Here, ρ_{3-C} is the three-dimensional density of a graphite wall, Δ is the interlayer distance between the graphene sheets of carbon wall, and z is the distances between an adsorbed molecule and the flat surface of carbon. The parameters of this potential are shown in Table 1. For all pore widths, the adsorption isotherms for the RSP model have a gradual uptakes at lower than $P/P_0 = 10^{-4}$ (see Figure 2b), although no such a gradual uptake is observed for the slit-shaped model. These results stem from the pore structure of the RSP model having a grooved structure. The adsorption isotherm on the RSP model width $w = 0.264$ nm shows this kind of uptake from $P/P_0 = 10^{-7}$ caused by the significant overlapping of interaction potential. Also, the simulated isotherms have a predominant second uptake above $P/P_0 = 10^{-4}$; the smaller the w value, the sharper the second uptake.

Figure 3 shows snapshots of nitrogen molecules in the pores of the RSP model as a function of the relative pressure and the pore width w. These snapshots show that the monolayer formation is completed below $P/P_0 = 10^{-2}$ for all cases. Adsorption in the smallest pore of $w = 0.264$ nm begins from the lowest relative pressure; a considerable number of molecules are adsorbed in the second layer even at a relative pressure of 10^{-2}. The snapshot variation from $P/P_0 = 10^{-2}$ to 10^{-1} suggests a remarkable filling effect, which corresponds to the second uptake of the simulated isotherms. This enhanced filling is associated with the cooperative filling caused by the aid of the strong interaction potential from the monolayer.[29]

The experimental adsorption isotherm on CMK-1 and the α_s-plot are shown in Figure 4, parts a and b, respectively. The isotherm coincides with one reported elsewhere.[30] The adsorption and desorption isotherms of CMK-1 overlap each other, showing little hysteresis. The adsorption isotherm features a hump from $P/P_0 = 0.25$ to 0.4 originating from adsorption in larger micropores or small mesopores and a gradual increase

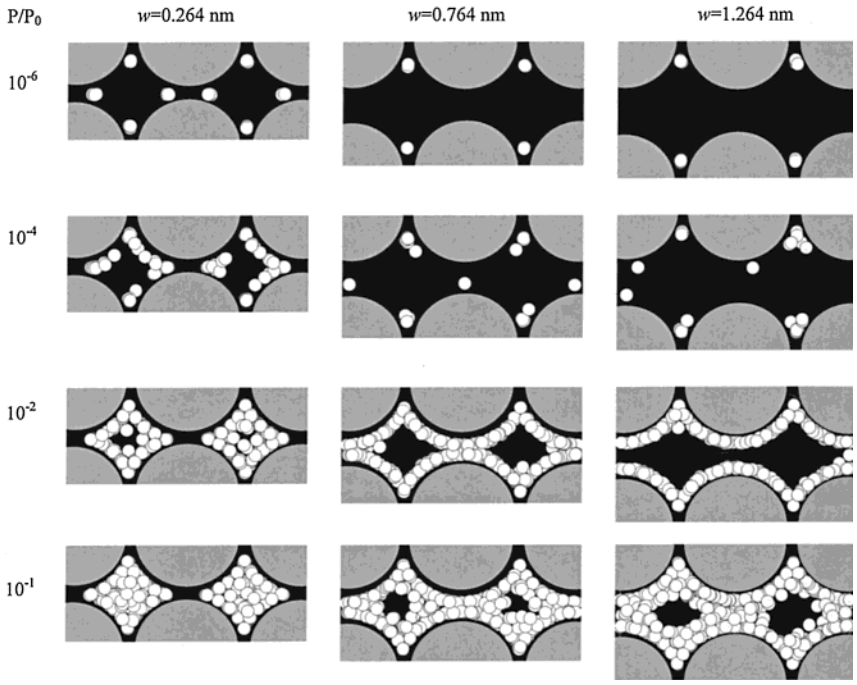

Figure 3. Side views of snapshots of adsorbed nitrogen in the RSP model at 77 K as functions of relative pressure and effective pore width.

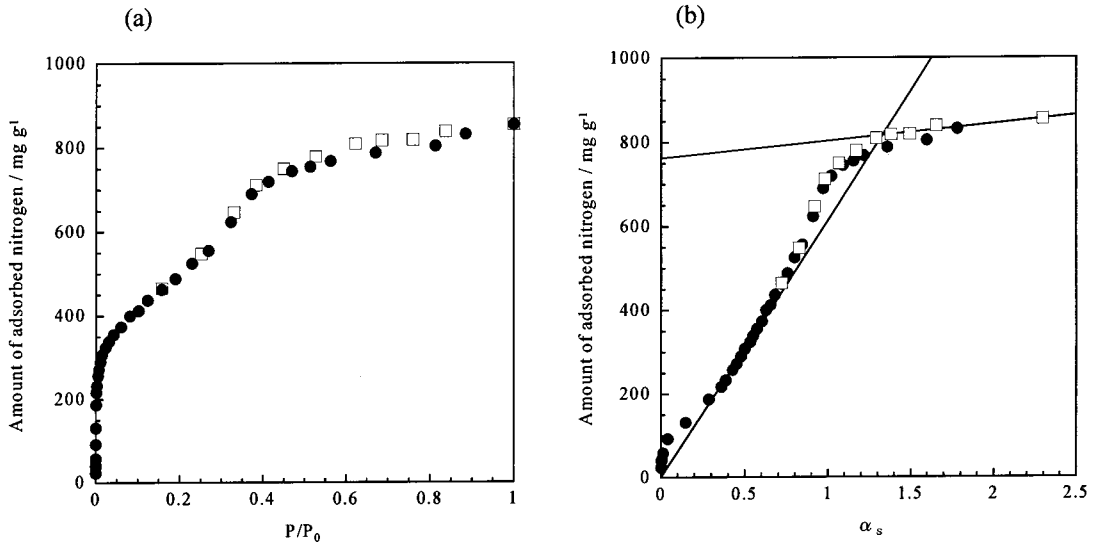

Figure 4. Adsorption (●) and desorption (□) isotherms of nitrogen on CMK-1 at 77 K (a) and high resolution α_s-plot for this isotherm (b).

TABLE 2: Pore Volume W_0^N, Total Surface Area a_α, and External Surface Area a_{ext} of CMK-1

W_0^N/mL g^{-1}	a_α/m^2 g^{-1}	a_{ext}/m^2 g^{-1}
0.94	1315	88

over $P/P_0 = 0.4$ due to adsorption on the wider pores and the external surface. A GCMC simulation study on the relationship between the α_s-plot and the PSD for the slit pores showed that two upward deviations of the α_s-plot below and above $\alpha_s = 0.5$ indicate the presence of bimodal PSD which range from 0.7 to 2.5 nm.[31] Therefore, CMK-1 should have a PSD from micropores to small mesopores. Both large micropores and small mesopores are predominant in CMK-1. The structural parameters of the micropores using the subtracting pore effect (SPE) method to analyze the α_s-plot are as shown in Table 2. The average pore width is calculated to be 1.5 nm if we assume the slitlike pore structure. This value is similar to that of MCM-48[32] analyzed with the Barrett-Joyner-Halenda (BJH) method, though this is different from the pore wall thickness of MCM-48 (ca. 1.0 nm) obtained by Schumacher et al.[33] This contradiction can be understood by the fact that the carbon precursor shrinks during carbonization, giving rise to the greater pore width than the pore wall thickness of MCM-48.

The simulated adsorption isotherms and the experimental one are compared in Figure 5. The GCMC-simulated and experimental isotherms are normalized by the adsorbed amounts at $P/P_0 = 1$ and the pore volume calculated by α_s-plot analysis, respectively. The multilayer adsorption on the external surface is subtracted from the observed isotherm using the SPE results. The simulated isotherm for $w = 1.264$ nm is in qualitative agreement with the experimental one over the whole range, though both do not overlap. Consequently, we can say that the RSP model for $w = 1.264$ nm can basically describe the fundamental adsorption process in pores of CMK-1. However this RSP model is still not realistic enough to describe in a quantitative way the detailed adsorption mechanism of nitrogen on CMK-1.

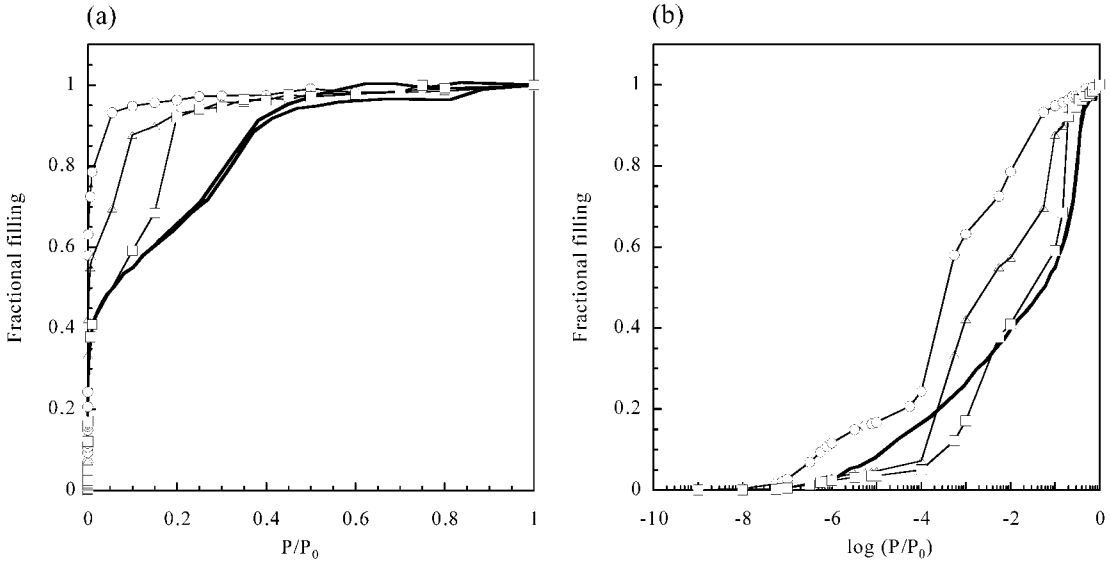

Figure 5. Fractional fillings of nitrogen on RSP models at 77 K: (○) $w = 0.264$ nm; (△) $w = 0.764$ nm; (□) $w = 1.264$ nm shown by relative pressure (a) and that of logarithm scale (b) for abscissa, respectively. The experimental result (bold solid line) was measured with gravimetric method at 77 K.

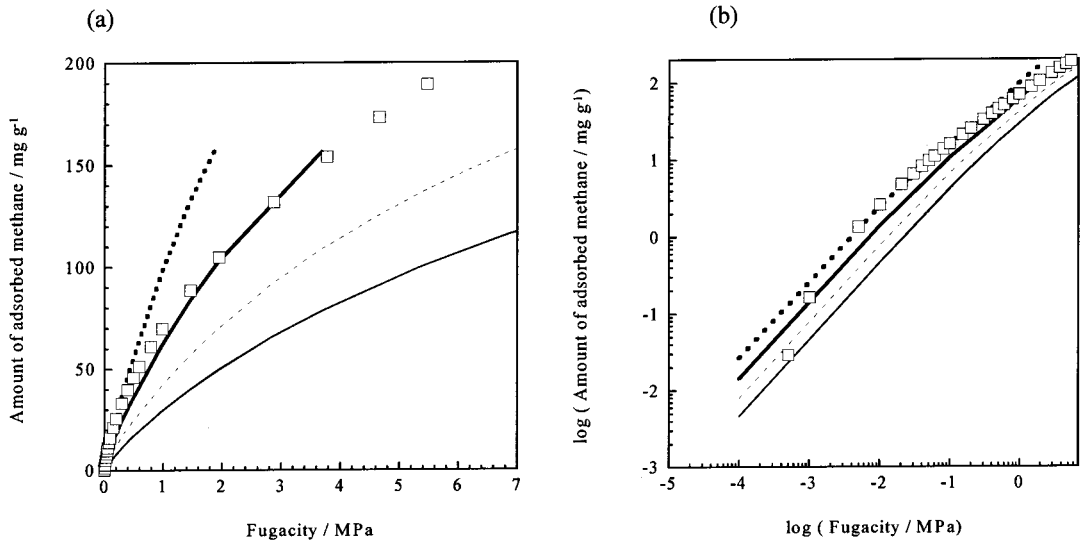

Figure 6. Simulated and experimental absolute amount of methane adsorbed on RSP model of $w = 1.264$ nm and CMK-1 at 303 K shown by fugacity and adsorbed density (a) and that of log−log plots (b): (fine solid line) $\epsilon_{sf} = 1.0\epsilon_{sf-0}$; (dashed line) $\epsilon_{sf} = 1.1\epsilon_{sf-0}$; (bold solid line) $\epsilon_{sf} = 1.2\epsilon_{sf-0}$; (dotted line) $\epsilon_{sf} = 1.3\epsilon_{sf-0}$; (□) experimental result on CMK-1.

Adsorption Mechanism of Supercritical Methane. Figure 6 shows both the simulated and the experimental absolute adsorption isotherms of methane at 303 K. We used the apparent particle density of 1.094 g/cm^3 calculated from the true density of graphite (2.267 g/cm^3) to convert the dimension of the simulated results for comparison. The simulations were carried out using different ϵ_{sf} values that were several times larger than the initial value of ϵ_{sf-0} (in this case $\epsilon_{sf-0}/k_B = 64.42$ K) calculated by using parameters shown in Table 1. A considerable good agreement is obtained for $\epsilon_{sf} = 1.2\epsilon_{sf-0}$ or $1.3\epsilon_{sf-0}$ at high and low pressure region, respectively. These results indicate that the enhancement of pore potential of CMK-1 is relatively larger, especially at low-pressure region because of the three-dimensional complex structure. The experimental data gradually approaches from the simulated result of $\epsilon_{sf} = 1.3\epsilon_{sf-0}$ to that of $\epsilon_{sf} = 1.2\epsilon_{sf-0}$ by increasing the fugacity. Hence the effect of pore potential is more emphasized at the beginning of adsorption process.

Figure 7 shows the snapshots of adsorbed methane for some fugacity points. The adsorption enhancement in the snapshots of $\epsilon_{sf} = 1.2\epsilon_{sf-0}$ is observed compared with the snapshots of $\epsilon_{sf} = 1.0\epsilon_{sf-0}$. The adsorption process of supercritical methane is different from that of nitrogen shown in Figure 3. In case of nitrogen adsorption at the boiling point, the filling proceeds with a kind of multilayer adsorption mechanism. However, such a regular multilayer formation is not observed in methane adsorption at 303 K. This is because the interaction between a methane molecule and the pore-wall of the RSP model is not enough to induce the regular multilayer adsorption; the real CMK-1 should have strong potential sites expressed by the RSP model.

The simulated adsorption isotherms can be compared with experimental results only when the saturate adsorbed amount or the pore volume of simulation cell can be solved accurately. The comparison of adsorption for supercritical fluids is very difficult because it is hard to define the saturated adsorption amount from both simulated and experimental data. In addition, the RSP model has a relatively complex structure compared with that of a slit and/or a cylindrical pore model. However, we can compare the properties of the adsorbed phase obtained

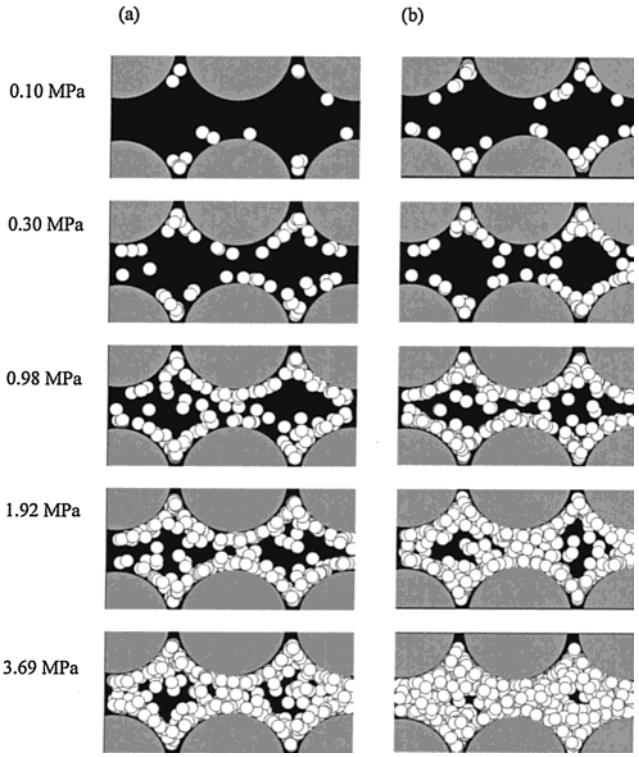

Figure 7. Side views of snapshots of adsorbed methane in the RSP model of $w = 1.264$ nm at 303 K as functions of fugacity: (a) $\epsilon_{sf} = 1.0\epsilon_{sf-0}$, (b) $\epsilon_{sf} = 1.2\epsilon_{sf-0}$.

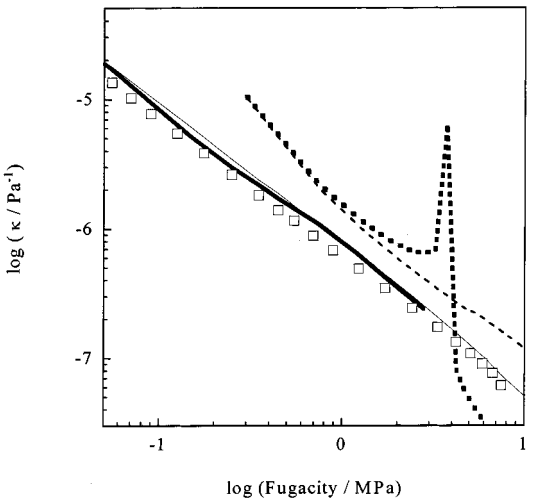

Figure 8. Simulated and experimental isothermal compressibility of adsorbed methane at 303 K: (bold solid line) on RSP model of $w = 1.264$ nm using $\epsilon_{sf} = 1.2\epsilon_{sf-0}$; (fine solid line) on RSP model of $w = 1.264$ nm using $\epsilon_{sf} = 1.0\epsilon_{sf-0}$; (□) on CMK-1; (dashed line) bulk methane at 300 K; (dotted line) bulk methane at 185 K.

from both simulation and experiment with those of the bulk phase by using the isothermal compressibility, because this value is only a function of fugacity. The isothermal compressibility is given by eq 6:

$$\kappa = -\frac{1}{V}\left(\frac{\partial V}{\partial P}\right)_T = \frac{1}{\rho}\left(\frac{\partial \rho}{\partial P}\right)_T \qquad (6)$$

Equation 6 can be applied to both simulated and experimental data. Figure 8 shows the simulated and experimental isothermal compressibility of adsorbed methane at 303 K. A rather good agreement is obtained for a wide pressure region on the simulated result of RSP model for $\epsilon_{sf} = 1.2\epsilon_{sf-0}$ and the experimental result. The upper deviation from the experimental results is observed for $\epsilon_{sf} = 1.0\epsilon_{sf-0}$ at low pressure. This is because of the differences of pore potential between two calculations as shown in Figure 6. The isothermal compressibility of the adsorbed methane is smaller than that of supercritical methane at 300 K.[34] On the other hand, the isothermal compressibility of bulk liquid methane at 185 K and over 5.5 MPa is estimated to be smaller than that of adsorbed methane at 303 K. Hence, we must conclude that the methane molecules confined in pores have an intermediate state between the supercritical and liquid states from the comparison of isothermal compressibility.

Acknowledgment. This work was funded by Grant-in-Aid for Scientific Research (Carbon Alloys) of the Japanese Government, and T.O. received support from the University of Edinburgh during his stay there.

References and Notes

(1) Rouquerol, F.; Rouquerol, J.; Sing, K. S. W. *Adsorption by Powders & Porous Solids*, Academic Press: London, 1999.
(2) Murata, K.; Kaneko, K. *Chem. Phys. Lett.* **2000**, *321*, 342.
(3) Miyawaki, J.; Kaneko, K. *Chem. Phys. Lett.* **2001**, *337*, 243.
(4) Conway, B. E. *Electrochemical Supercapacitors: Scientific Fundamentals and Technological Applications*, Kluwer Academic/Plenum Publishers: New York, 1999.
(5) Iiyama, T.; Nishikawa, K.; Otowa, T.; Kaneko, K. *J. Phys. Chem.* **1995**, *99*, 10075.
(6) Iiyama, T.; Nishikawa, K.; Suzuki, T.; Kaneko, K. *Chem. Phys. Lett.* **1997**, *274*, 152.
(7) Ohkubo, T.; Iiyama, T.; Nishikawa, K.; Suzuki, T.; Kaneko, K. *J. Phys. Chem. B* **1999**, *103*, 1859.
(8) Ohkubo, T.; Yang, C.-M.; Raymundo-Piñero, E.; Linares-Solano, A.; Kaneko, K. *Chem. Phys. Lett.* **2000**, *329*, 71.
(9) Kaneko, K. *Carbon* **2000**, *38*, 287.
(10) Ohkubo, T.; Kaneko, K. *Colloids and Surf. A* **2001**, *187−188*, 177.
(11) Kyotani, T.; Tsai, L.-F.; Tomita, A. *Chem. Mater.* **1996**, *8*, 2109.
(12) Ryoo, R.; Joo, S. H.; Jun, S. *J. Phys. Chem. B* **1999**, *103*, 7743.
(13) Kruk, M.; Jaroniec, M.; Ryoo, R.; Joo, S. H. *J. Phys. Chem. B* **2000**, *104*, 7960.
(14) Jun, S.; Joo, S. H.; Ryoo, R.; Kruk, M.; Jaroniec, M.; Liu, Z.; Ohsuna, T.; Terasaki, O. *J. Am. Chem. Soc.* **2000**, *122*, 10712.
(15) Joo, S. H.; Jun, S.; Ryoo, R. *Microporous and Mesoporous Mater.* **2001**, *44−45*, 153.
(16) Ryoo, R.; Joo, S. H.; Kruk, M.; Jaroniec, M. *Adv. Mater.* **2001**, *13*, 677.
(17) Joo, S. H.; Choi, S. J.; Oh, I.; Kwak, J.; Kiu, Z.; Terasaki, O.; Ryoo, R. *Nature* **2001**, *412*, 169.
(18) Beck, J. S.; Vartuli, J. C.; Roth, W. J.; Leonowicz, M. E.; Kresge, C. T.; Schmitt, K. D.; Chu, T. T.-W.; Olson, D. H.; Sheppard, E. W.; McCullen, S. B.; Higgins, J. B.; Schlenker, J. L. *J. Am. Chem. Soc.* **1992**, *114*, 10834.
(19) Frenkel, D.; Smit, B. *Understanding Molecular Simulation: From Algorithms to Applications*, Academic Press: San Diego, **1996**.
(20) Sonwane, C. G.; Bhatia, S. K. *J. Phys. Chem. B* **2000**, *104*, 9099.
(21) Steele, W. A.; Bojan, M. J. *Adv. Colloid Interface Sci.* **1998**, *76−77*, 153.
(22) Peng, D.-Y.; Robinson, D. B. *IEC Fundam.* **1976**, *15*, 59.
(23) Sandler, S. I. *Chemical and Engineering Thermodynamics*, Willey & Sons: New York, 1999.
(24) Kaneko, K.; Ishii, C. *Colloids Surf.* **1992**, *67*, 203.
(25) Setoyama, N.; Suzuki, T.; Kaneko, K. *Carbon* **1998**, *36*, 1459.
(26) Murata, K.; Miyawaki, J.; Kaneko, K. *Carbon* **2002**, *40*, 425.
(27) Kaneko, K.; Cracknell, R. F.; Nicholson, D. *Langmuir* **1994**, *10*, 4640.
(28) Steele, W. A. *Surf. Sci.* **1973**, *36*, 317.
(29) Ohba, T.; Suzuki, T.; Kaneko, K. *Chem. Phys. Lett.* **2000**, *38*, 1879.
(30) Kruk, M.; Jaroniec, M.; Ryoo, R.; Joo, S. H. *J. Phys. Chem. B* **2000**, *104*, 7960.
(31) Setoyama, N.; Suzuki, T.; Kaneko, K. *Carbon* **1998**, *36*, 1459.
(32) Fröba, M.; Köhn, R.; Bouffaud, G. *Chem. Mater.* **1999**, *11*, 2858.
(33) Schumacher, K.; Ravicovitch, P. I.; Chesne, A. D.; Neimark, A. V.; Unger, K. K. *Langmuir* **2000**, *16*, 4648.
(34) Sychev, V. V.; Vasserman, A. A.; Zagoruchenko, V. A.; Spiridonov, G. A.; Tsymarny, V. A. *Thermodynamic Properties of Methane*, Hemisphere Pub. Corp., Washington D. C., **1987**.